Proc. Inst. Electrostat. Jpn.

静電気学会誌, **20**, 4 (1996), 238-246

論　　文

Induced Current Characteristics of Square Probe Placed at Ground Level in a Parallel DC and AC Lines-to-Plate Electrode System

Marsul SIREGAR,* Noriyuki HAYASHI,** Junya HASHIMOTO* and Katsuo ISAKA**

(Received February 13, 1996)

Laboratory investigation on the characteristics of the current induced in conductive objects placed at ground level in electrical environment where the ac electric field and dc ion field concurrently exist is conducted by using a parallel ac and dc lines-to-plate electrode system. Experimental results show that the current induced in the current probe is reduced after the inception of the corona discharge on the dc line, and that the amount of the induced-current reduction greatly depends on the dc line voltage and the frequency of the ac line voltage as well as the probe locations. It is also found that the induced current contains some harmonics of several orders, especially 2nd to 4th order harmonics. Two models taking into account the space charge vibration due to the ac electric field and ac field shielding effect due to the space charge are successfully introduced to qualitatively explain the experimental results, namely to demonstrate how the magnitudes and orders of the harmonics contained in the induced current are affected.

1. Introduction

Long distance and high voltage dc transmission has received wide attention because of its technical and economical advantages. However, construction of new lines and obtaining new right-of-ways for the lines have become very difficult due to the public concern over the environmental effects. New options for increasing the efficiency of power transmission and overcoming the difficulties in obtaining new right-of-ways are to build a hybrid ac and dc line by converting an existing the hvac line to a hvdc line or by constructing a new hvdc line in an existing corridor.

Since 1981,[1] a lot of experimental and computational investigations regarding ac/dc hybrid lines and corridors have been conducted to date using full scale and reduced-scale lines. The mutual interaction due to close proximity of ac and dc conductors affects the corona performance on both lines[1-3] and the electrical environment under the lines such as the dc electric field and ion current distribution.[4-6]

From the electrical point of view, the inter-electrode space under the hybrid lines is a complex environment where the ac electric field and dc ion flow field concurrently exist. Most of the research mentioned above are concerned with phenomena regarding to the dc ion field, however few investigations on phenomena regarding the ac electric field have been conducted and reported.

The present contribution demonstrates experimental results obtained by laboratory investigation on the characteristics of the current induced in conductive objects placed in electrical environments where the ac electric field and dc ion field concurrently exist. The experimental results will be discussed based on the simple models that take into account the space charge vibration caused by the ac electric field and the ac flux shielding effect of the space charge.

2. Description of Experimental Setup and Instrumentations

All experiments in the present investigation were conducted using a parallel ac and dc lines-to-plate electrode system diagrammed in Fig. 1. The plate electrode of 2 m×4 m in size is made of four aluminum plates, and supported by a wooden frame of the height

Keywords : AC field, DC ion flow field, induced current, AC field shield, ion vibration

* Graduate School of Engineering, The University of Tokushima, Tokushima, 770 Japan

** Faculty of Engineering, The University of Tokushima, Tokushima, 770 Japan

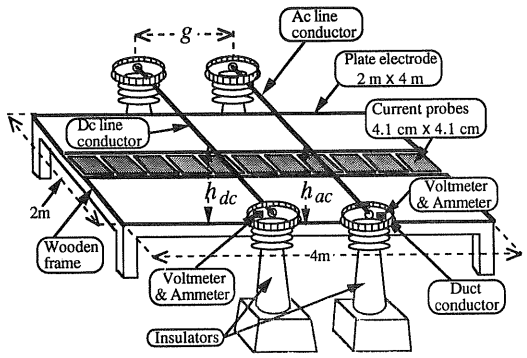

Fig. 1 Schematic diagram of the experimental setup.

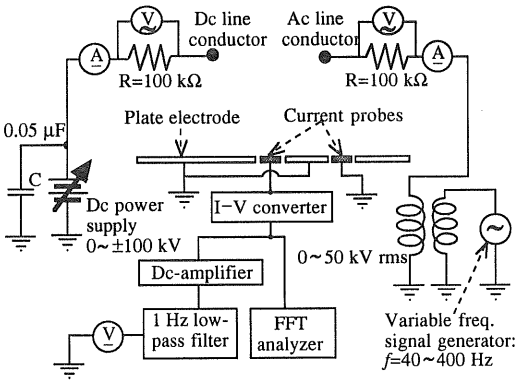

Fig. 2 Ac and dc power supply systems and current measurement instrumentation.

1.16 m. The plate electrode is solidly grounded. Ninety four pieces of the square brass plate of 4.1 cm×4.1 cm in size are placed in series, being flush with the plate electrode, and employed as current probes. The current probes are separated from each other and from the plate electrode by an air gap of 1 mm.

A steel pipe of diameter 25.5 mm and a copper wire of 1 mm in diameter are used as the ac and dc line conductors, respectively, and are horizontally situated in parallel with each other with the spacing of g at a height of h above the plate electrode. The thick conductor is employed for the ac line to satisfy the following situations: one is to have no corona discharge occur on it under all experimental conditions applied, and the other to achieve the ac electric field strengths as low as those under practical ac/dc hybrid lines. Meanwhile the thin dc conductor is used as a stable source of ion in the inter-electrode space.

Figure 2 shows the electric circuits of both ac and dc power supply systems to the line electrodes, and diagrams the instrumentation to measure the current to the current probes. The dc power supply can energize the dc conductor up to ± 100 kV with the rated current of 1 mA, while the ac power transformer can produce a voltage of 0 to 50 kV_{rms} with the rated current of 10 mA. Frequency of the ac applied voltage is varied from 40 to 400 Hz by changing the frequency of the voltage signal fed to the ac power transformer, the voltage signal being generated by a variable frequency sinusoidal voltage generator.

The current probes placed at ground level sense the induced current and the ionic current, both currents concurrently flowing into the current probes. Probe current signals i_p are converted to the corresponding voltage signals v_p by using an I-V converter circuit with the variable gains of 10^4, 10^6 and 10^8. The voltage signal v_p is fed to the ONO-SOKKI CF-1200 handheld FFT analyzer to measure the magnitudes and waveforms of i_p. The magnitude of the dc component in i_p is generally much smaller than the ac component, so that the current measuring systems using the FFT analyzer mentioned above is inadequate to measure the magnitude of the dc component in i_p. Hence v_p is magnified by a dc amplifier by 10 to 100, and then fed to the dc voltage measuring system consisted of a 1 Hz low-pass filter circuit and a dc voltmeter. The dc amplifier has an internal 10 Hz low-pass filter, so that only the dc component in v_p is amplified at this stage. The probe current density J_p is simply defined as $J_p = I_p/S$, where I_p is the total probe current and S the area of the current probe.

To measure the ac component I_{ac-1} contained in the line current, a 100 kΩ resistor is inserted in series between the power supply and line conductor, and the voltage drop across it is measured by a battery-operated digital ac voltmeter. Furthermore a moving-coil type ammeter is connected in series with the resistor to measure the dc component I_{dc-1} contained in the line current. All of those meters are placed on the top of the electrical insulators supporting the line conductors, and capped by metal duct conductors to lessen the electric field concentration around them.

3. Experimental Results

Under various geometrical and electrical conditions, magnitudes and waveforms of the induced currents in the current probes are measured at five different locations P_1–P_5 as indicated in Fig. 3. No experiment with a 60 Hz ac line voltage was conducted to avoid unexpected interference from the ambient wiring system and electric apparatus.

In this chapter, shown are experimental results obtained under the geometrical configuration of $h=0.31$ m and $g=0.63$ m with the ac line voltage V_{ac-1} of 50 Hz. With V_{ac-1} up to 50 kV_{rms}, no corona discharge on the ac line conductor occurred in the present investigation.

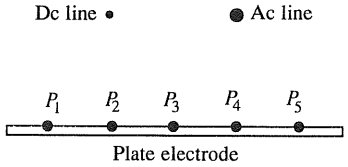

Fig. 3　Locations of the current probes where induced current is examined.

3. 1　Change in Induced Current Density

Magnitudes of the fundamental components of the induced current density J_{ac-p}, e.g. 50 Hz components in the present case, obtained at the location P_2 are plotted in Fig. 4 as a function of the negative dc line voltage

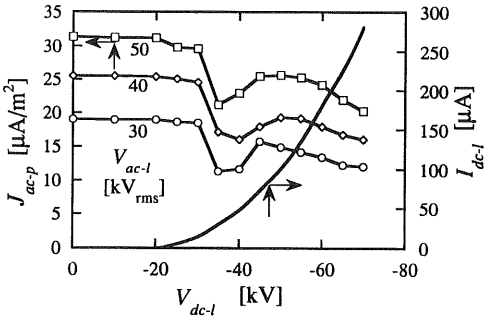

Fig. 4　Dependency of J_{ac-p} and I_{dc-l} on V_{dc-l} at location P_2.

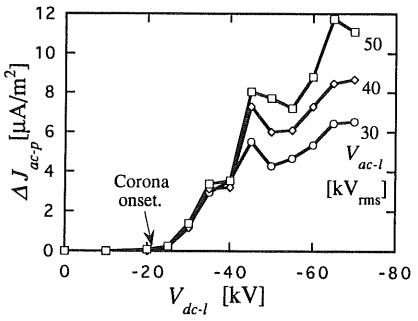

(a) Location P_1.

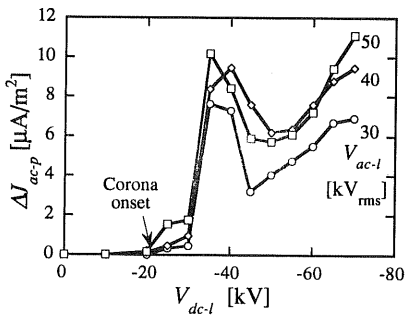

(b) Location P_2.

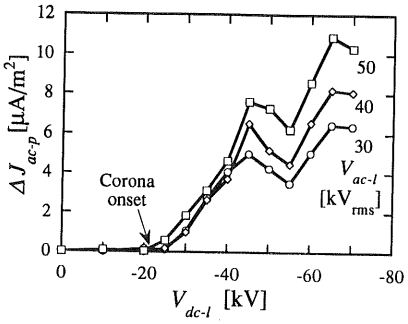

(c) Location P_3.

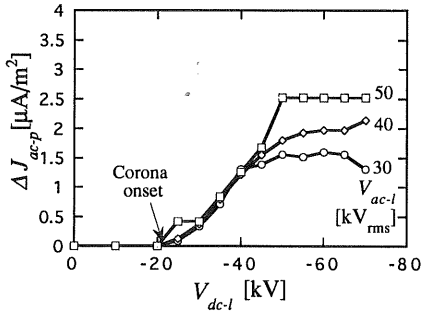

(d) Location P_4.

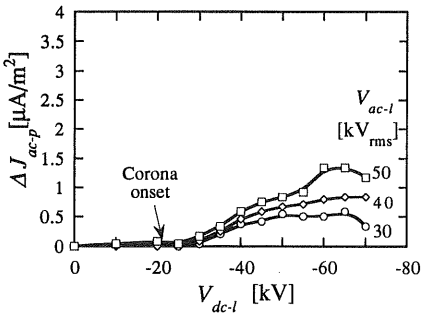

(e) Location P_5.

Fig. 5　$V_{dc-l}-\Delta J_{ac-p}$ characteristics for various ac line voltages.

V_{dc-1} for various ac line voltages V_{ac-1} of 30 kV_{rms}, 40 kV_{rms} and 50 kV_{rms}. The dc line current I_{dc-1} flowing in the dc line is also shown in Fig. 4 as a function of V_{dc-1}. Figure 4 shows that the corona discharge on the dc line initiates at V_{dc-1} of about 22 kV, and that both the dc corona inception voltage and I_{dc-1} values are almost independent of V_{ac-1} under the present experimental conditions.

It is found from Fig. 4 that the values of J_{ac-p} decreases as V_{dc-1} increases after the dc corona inception. Although those reductions of J_{ac-p} against V_{dc-1} are obtained at all probe locations examined, the characteristics of the J_{ac-p} reduction greatly depend on the probe locations.

The amount of the J_{ac-p} reduction, ΔJ_{ac-p}, that is referred to J_{ac-p} with no ions in the inter-electrode space, is plotted in Fig. 5 as a function of V_{dc-1} for various probe locations and V_{ac-1}. Inspection of Fig. 5 indicates that ΔJ_{ac-p} obtained for higher V_{ac-1} are larger at all probe locations, and that the way how J_{ac-p} decreases is almost independent of V_{ac-1}. It is also found that ΔJ_{ac-p} at the locations P_1, P_2 and P_3 are larger than those at P_4 and P_5. The dc ion current densities J_{dc-p} are 60.6 $\mu A/m^2$ on the probe at the location P_1, 202 $\mu A/m^2$ at P_2, 51.0 $\mu A/m^2$ at P_3, 5.59 $\mu A/m^2$ at P_4 and 0.84 $\mu A/m^2$ at P_5.[6] It will be stated that the degree of the J_{ac-p} reduction closely corresponds to the ion current density near the probe under discussion.

Although Figs. 4 and 5 demonstrate the experimental results obtained under the limited geometrical and electrical conditions, almost the same conclusions as those mentioned above can be drawn in the case of the different geometrical configuration of $h=0.31$ m and $g=0.98$ m and/or the positive V_{dc-1}.

3. 2 Waveforms of Induced Current

Figure 6 shows the waveforms v_{ac-1} of V_{ac-1} and corresponding induced current signal i_{ac-p} measured at the location P_2. All waveforms plotted in Fig. 6 are obtained with a constant V_{ac-1} of 30 kV_{rms} and various negative V_{dc-1} up to -45 kV. Results of the Fourier transformation of v_{ac-1} indicate that v_{ac-1} includes negligible amount of higher order components, and hence it is concluded that the ac line voltage is almost a pure sinusoidal voltage.

Inspection of Fig. 6 indicates that, after the inception of the dc corona discharge, i_{ac-p} includes a lot of spikes and its waveform is distorted. It is also seen that the spike signals take place during only the positive cycles of v_{ac-1} for smaller V_{dc-1}, and during both positive and negative cycles of v_{ac-1} for higher V_{dc-1}. Those spike signals are possibly attributed to the intermittent magnification of the dc corona activity by the periodical change in V_{ac-1}, resulting in the sharp change in the electric field strength on the current probes, and hence in the induced current in them.

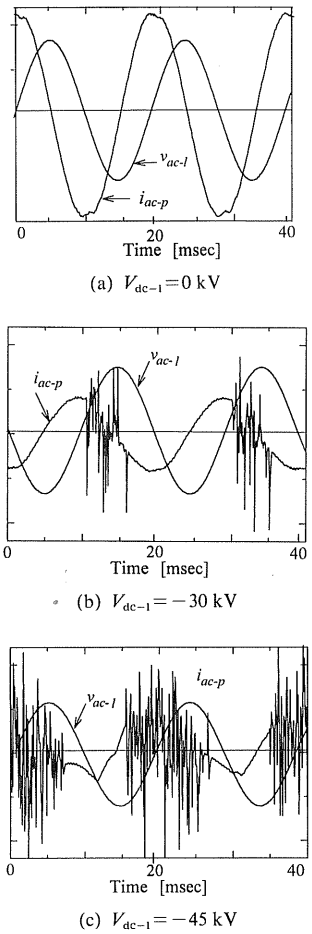

Fig. 6 Waveforms of the induced current i_{ac-p} and the ac line voltage v_{ac-1}.

Under the present experimental conditions the positive corona discharge is quite silent and few spike signals appears in the waveform of i_{ac-p} for all V_{dc-1} applied in the case of the positive line voltage.

3. 3 Harmonics Contained in Induced Current

As is seen in Fig. 6, besides the signal spikes due to the corona activity on the dc line, the induced current signals i_{ac-p} on the current probes are distorted as V_{dc-1} increases, and consequently the higher order harmonics are included in the i_{ac-p} signals.

Figure 7 shows how the magnitudes of each harmonic components contained in the i_{ac-1} signals vary with the negative V_{dc-1}. All data illustrated in Fig. 7 are obtained at the location P_2 with a constant V_{ac-1} of 30 kV_{rms}.

It is seen from Fig. 7 that, for the negative V_{dc-1}

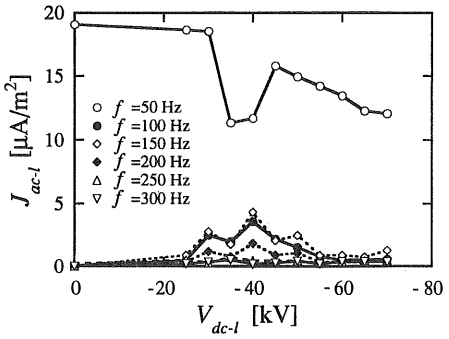

Fig. 7　Magnitudes of the harmonic components contained in induced current.

between −25 kV and −55 kV, the magnitude of the fundamental component dramatically decreases, and relatively significant amount of harmonics, in particular 2nd to 4th order harmonics, are included in the i_{ac-p} signals. Further increase in V_{dc-l}, in turn, decreases the magnitude of the harmonics of all orders. The i_{ac-l} signals measured at the other locations also include the various orders of the harmonics; however the amount of harmonic contents beneath the dc line is larger than those at the other locations.

Almost the same harmonic characteristics are obtained in the case of the positive line voltage.

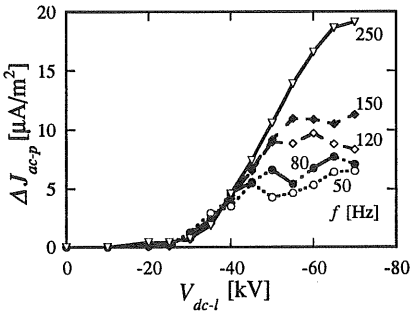

(a) Location P_1

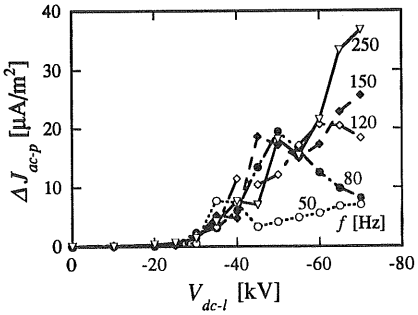

(b) Location P_2

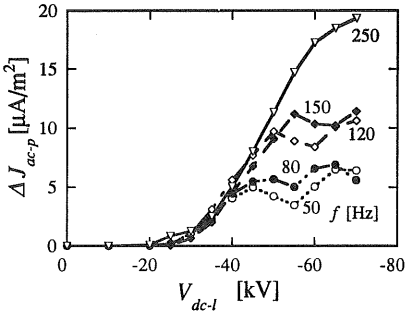

(c) Location P_3

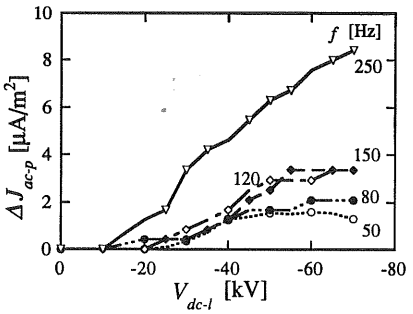

(d) Location P_4

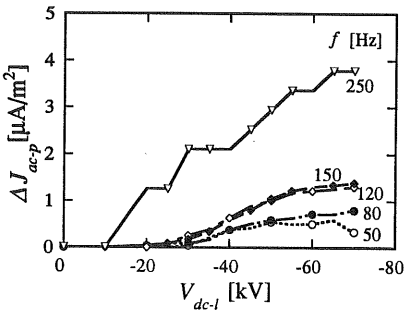

(e) Location P_5

Fig. 8　$V_{dc-l}-\Delta J_{ac-p}$ characteristics for various frequencies of ac line voltage.

3. 4 Effects of Frequency of Ac Line Voltage on Induced Current

As stated in the previous section 3.1, the increase in V_{dc-l} causes the decrease in the magnitude of the induced current of fundamental frequency. To examine those phenomena, supplemental experiments were designed and conducted by changing the frequency f of V_{ac-l} with the constant values of $V_{ac-l}=30\ kV_{rms}$ and the constant negative V_{dc-l} of -30 kV for the geometrical configuration of $g=0.63$ m and $h=0.31$ m.

Figure 8 shows the dependency of the amount of the J_{ac-p} reduction, ΔJ_{ac-p}, on the negative V_{dc-l} measured at the locations P_1-P_5 when f is varied from 50 Hz to 250 Hz.

It is seen from Fig. 8 that J_{ac-p} monotonously decreases as V_{dc-l} increases for all frequencies examined, except for those at the location P_2. The values of ΔJ_{ac-p} obtained at the location P_2 behave in a complex way as f and V_{dc-l} vary, in particular for V_{dc-l} between -35 kV to -60 kV. Figure 8 also indicates that the higher frequency makes ΔJ_{ac-p} larger, and ΔJ_{ac-p} is larger under the dc line (the locations P_1-P_3) than under the ac line (the locations P_4 and P_5). Based on the profile of the dc ion current density on the current probes,[6] it will be stated, as well as in the case indicated in Section 3.1, that the amount of the J_{ac-p} reduction closely corresponds to the ion current density in the probe concerned.

Almost the same ΔJ_{ac-p} characteristics against f and V_{dc-l} are obtained in the case of the positive V_{dc-l}.

4. Discussions

4. 1 Induced Current by Vibration of Space Charge Due to Ac Field

Space charges with the same polarity as the dc line fill the inter-electrode space after the inception of the dc line corona. Those space charges experience the electric force attributed to both the ac and dc electric fields simultaneously, and the ac electric field makes the space charges vibration in the interelectrode space.

Drawn in Fig. 9(a) is a cloud of space charges of the electric charge q that vibrates in the vicinity of the current probe. Total electric field E_{total} on the current probe is given by $E_{total}=E_{ion}+E_{ac-l}$, here E_{ion} is due to the vibration of the charge q and E_{ac-l} is due to the ac line voltage.

Providing that both the space charge cloud and current probe are exposed to a uniform ac electric field E_{ac0} of the magnitude E_{ac0} and angular frequency ω, E_{ac0} being vertical to the current probe and equivalent to E_{ac-l}, the magnitude E_{ion} of the electric field E_{ion} and the induced current i_p in the current probe due to E_{total} are given by Eqs. (1) and (2), respectively.

$$E_{ion}=\frac{q}{2\pi\varepsilon}\frac{1}{\left\{r_0+\frac{\mu E_{ac0}}{\omega}(1-\cos\omega t)\right\}^2} \tag{1}$$

$$i_p=\varepsilon S\frac{d}{dt}(E_{ion}+E_{ac-l})$$

$$=\frac{\mu qS}{\pi}\frac{-E_{ac0}\sin(\omega t)}{\left\{r_0+\frac{\mu E_{ac0}}{\omega}(1-\cos\omega t)\right\}^3}-k_1\omega\cos\omega t \tag{2}$$

Here r_0 is an initial height of the space charge above the probe, μ the ion mobility, ε the permittivity of free space, S the probe area, and k_1 a constant depending on the geometrical configuration of the line system.

The induced current expressed in Eq. (2) is analyzed by applying the Fourier transformation, and a typical result is plotted in Fig. 10. It is clear from Fig. 10 that the magnitude of the fundamental component of i_p is greater than a unit and both even and odd order harmonics are included. Almost the same characteristics of i_p as shown in Fig. 10 are obtained for other amplitudes and frequency of the space charge vibration. Consequently it is found that the vibration of space charges in the inter-electrode space causes the enhancement of the magnitude of the fundamental component of i_p, and generates both the even- and odd-order harmonics.

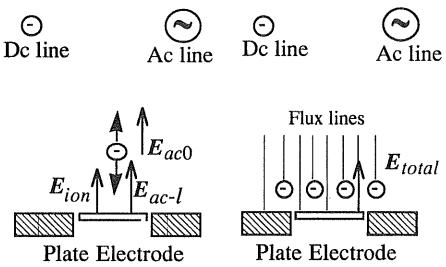

(a) Space charge vibration (b) Shielding of flux

Fig. 9 Proposed models to explain the experimental results.

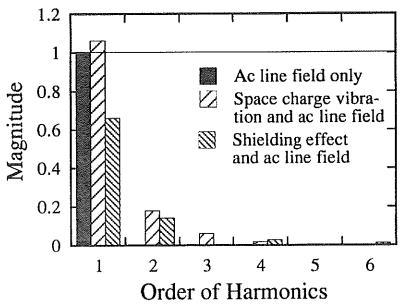

Fig. 10 Magnitude and orders of harmonics contained in i_p resulting from the space charge vibration and field shielding effect.

4. 2 Induced Current by Shielding of AC Flux Due to Space Charge

Figure 9(b) schematically illustrates the shielding of the ac field flux by the negative space charges near the current probes, resulting in the decrease in the electric field strength on the current probe. This shielding effect takes place only when the polarity of the ac line voltage is opposite to that of the space charges, e.g. only during the positive cycle of V_{ac-1} when the negative space charges exist.

The shielding effect generates an asymmetrical waveform of $\boldsymbol{E}_{total}$ on the current probe, i.e. in general the reduction of the ac field magnitude during either positive or negative cycle only. Providing that the magnitude of $\boldsymbol{E}_{total}$ is expressed by Eqs. (3) and (3′), the induced current due to $\boldsymbol{E}_{total}$ is given by Eqs. (4) and (4′). The typical waveforms of i_p obtained by the practical experiments using the positive dc line and by the theoretical calculation based on the ac field shielding effects are drawn in Figs. 11(a) and 11(b), respectively, as a function of time in an arbitrary scale as well as the ac line voltage v_{ac-1}. The waveform of the induced current in Fig. 11(a) is obtained by omitting high frequency components larger than 1 kHz.

$$E_{total}=E_{ac0}\sin(\omega t) \quad \text{(for a certain cycle of } \boldsymbol{E}_{total}) \tag{3}$$

$$=nE_{ac0}\sin(\omega t) \quad \text{(for another cycle of } \boldsymbol{E}_{total}), \tag{3′}$$

$$i_p=\omega E_{ac0}\sin(\omega t) \tag{4}$$

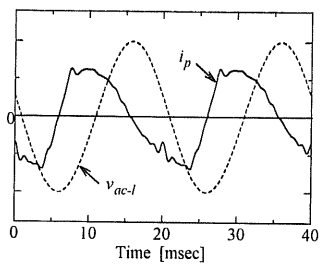

(a) Measured waveform (V_{dc-1}=45 kV).

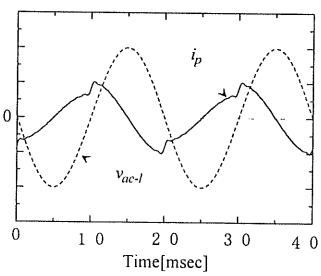

(b) Estimated one based on shielding effect.

Fig. 11　Waveforms of i_p and ac line voltage V_{ac-1}.

$$=n\omega E_{ac0}\sin(\omega t) \quad \text{(for a certain cycle of } \boldsymbol{E}_{total}) \tag{4′}$$

$$\text{(for another cycle of } \boldsymbol{E}_{total}).$$

where n is the ratio of the magnitude reduction of E_{total}.

The induced current expressed in Eqs. (4) and (4′) is analyzed for various magnitudes of the reduced cycles by applying the Fourier transformation. A typical result obtained for $n=1/3$ is shown in Fig. 10.

Figure 10 shows that the magnitude of the fundamental component is smaller than a unit and only even-order harmonics are included in the i_p signals generated by the space charge shielding effect. Hence it is concluded that the field shielding effect caused by the space charges decreases the magnitude of the fundamental component of i_p and generates only the even-order harmonics.

It is also found that the larger the reduction of the field magnitude of either cycle is, the more significant the reduction of the magnitude of the fundamental component of i_p becomes and the larger the magnitudes of the even-order harmonics become. Namely it will be safe to say that higher density of space charges around the probes causes more significant reduction of the magnitude of the fundamental component of i_p.

4. 3 Space Charge Density at Ground Level

It is known[7] that the electric field E and ion current density J at ground level in a single-line to plane electrode system are expressed in the form of Eqs. (5) and (6), respectively.

$$E=\frac{E_m}{(1+x^2)^{0.78}}, \tag{5}$$

$$J=\frac{J_m}{(1+x^2)^{2.4}}, \tag{6}$$

Here E_m and J_m are maximum values of E and J beneath the dc line, respectively, and x the normalized horizontal distance referred to the line height h.

By employing Eqs. (5) and (6), it is expected in the present case that the ion density ρ is given by the following equation (7).

$$\rho=\frac{J}{\mu E}\propto\frac{1}{(1+x^2)^{1.62}} \tag{7}$$

Equation (7) indicates that the ion density is the highest beneath the dc line and monotonously decreases as x increases.

4. 4 Discussions Based on Models

If both the vibration of the space charge by the ac electric field and the shielding effects of the ac electric field by the space charges mentioned above are introduced as a possible mechanisms, experimental results described in the previous chapter 3 will be

qualitatively explained as follows.

The field shielding effect by the space charge depends on the ion density near the current probe, and hence becomes more significant as the dc line voltage and corresponding space charge density increases. As stated in the previous section 4.3, the ion density is expected to be maximum at the location P_2 and gradually to decrease from the locations P_3 to P_5. This behavior of the ion density profiles corresponds to the change in the amount of the J_{ac-p} reduction described in Figs. 5 (a)–5(e) and 8(a)–8(e) when the location of the probes are changed. Furthermore the increase in the dc line voltage also lessens the effect of the space charge vibration, resulting from the enhancement of the dc electric field experienced by the space charges and consequent enhancement of the dc drift velocity of the space charge.

On the other hand the amplitude of the space charge vibration becomes smaller when the frequency of the ac line voltage, i.e. the frequency of the ac electric field experienced by the space charge, increases, resulting in the mitigated influence of the space charge vibration on the induced current.

Consequently it is expected that both mechanisms simultaneously take place for the intermediate dc voltage and/or the low frequency of the ac line voltage, resulting in the non-monotonous decrease in the induced current and the introduction of the even and odd order harmonics to the waveform of the induced current. However, for the high dc line voltage and/or the high frequency of the ac line voltage, the effect of the space charge vibration diminishes and the shielding effect becomes predominant, which cause the monotonous decrease in the induced current.

The mechanism based on the flux shielding effect is also supported by the similarity of the waveforms of i_p between the practical ones shown in Fig. 11(a) and theoretical ones shown in Fig. 11(b).

4. 5 Application under Practical Ac/Dc Lines

One of the common applications of the induced current under ac/dc transmission lines is the measurement of the ac electric field strength distributions at ground level. Capacitive probes are used in an ac field filled with space charges emitted from the dc line.

It is expected that, under practical ac/dc lines, the ion current density will be below 100 nA/m^2, and the ac electric field less than 10 kV/m_{rms}.[1,4] Similar electrical environments are obtained at the location P_5 in the present investigation. Experimental data obtained at P_5 such as Fig. 5(e) indicate that the amount of the J_{ac-p} reduction, ΔJ_{ac-p}, is less than 1% of the absolute induced current density in the current probe. Hence it will be concluded that the effects of the space charges on the reduction of the induced current in the conductive objects are negligible under those electrical environments mentioned above.

Therefore it can be said that, under the practical ac/dc transmission lines, the existence of space charges near the ac field probes, which are electrically grounded and used to sense the ground-level ac field strength, has less influence on the ac field measurements.

If should be, however, noted that the accumulation of space charges on conductive objects with non-zero impedance to ground and resultant change in their dc potential may change the induced current characteristics in them. Consequently their impedance to ground should be taken into consideration to determine the induced current characteristics in such objects even under the practical ac/dc transmission lines.

5. Conclusions

Laboratory investigations on the characteristics of the current induced in conductive objects placed in electrical environments where the ac electric field and dc ion field concurrently exist are conducted. Those investigations used a parallel ac and dc lines-to-plate electrode system.

Experimental results indicate that the current induced in the conductive objects decreases after the inception of the dc corona discharge, and that the amount of the current reduction greatly depends on both the dc line voltage and the frequency of the ac line voltage. It is also indicated that the induced probe current contains harmonics of several orders, especially 2nd to 4th order harmonics. It is finally pointed out from those experimental results that effects of the space charges on the induced current in the conductive objects which is electrically grounded are significant in an ac field which is rich of space charges.

Two simple models are successfully introduced to qualitatively demonstrate how the magnitudes and orders of the harmonics contained in the induced current are affected by both the vibration of the space charges in the vicinity of the current probes due to the ac electric field, and the reduction of the ac electric field strength on the current probes due to the shielding effect of the space charge. No quantitative explanation of the experimental results, however, is executed for lack of some essential data such as dc electric field strength near the current probes.

For the practical ac/dc lines which supply an ac electromagnetic environment with space charges at ground level, it is concluded that the electrically grounded probes at ground level are able to be employed to measure the ground-level ac field distribution with a reasonable error. It is also noted that the impedance to ground should be taken into considera-

tion to determine the induced current characteristics of insulated objects like human body with insulating shoes even under the ac/dc transmission lines.

References

1) V.L. Chartier, S.H. Sarkinen, R.D. Stearns and A.L. Burn : IEEE Trans. Power Appar. Syst., **PAS-100** (1981) 72
2) M.R. Raghuuveer : J. Electrostat., **22** (1989) 279
3) T. Zhao, S.A. Sebo and D.G. Kasten : *IEEE/PES Summer Meeting, 95 SM 407-7 PWRD*, p. 1, (1995)
4) P. Sarma Maruvada and S. Drogi : IEEE Trans. Power Delivery, **3** (1988) 1165
5) B.A. Clairmont, G.B. Johnson, L.E. Zaffanella and S. Zelingher : IEEE Trans. Power Delivery, **4** (1989) 1388
6) M. Siregar, N. Hayashi, K. Isaka, J. Hashimoto and Y. Yokoi : *Proceedings of the 11th International Conference on Gas Discharge and Their Applications, Tokyo*, Vol. I, p. 196 (1995)
7) M. Hara, N. Hayashi, K. Shiotsuki and M. Akazaki : IEEE Trans. Power Appar. Syst., **PAS-101** (1982) 803